

# Estimation of the fourth-order dispersion coefficient $\beta_4$

Jing Huang (黄菁)<sup>1\*</sup> and Jianquan Yao (姚建铨)<sup>2</sup>

<sup>1</sup>Physics Department, South China University of Technology, Guangzhou 510640, China

<sup>2</sup>College of Precision Instrument and Opto-Electronics Engineering, Tianjin University, Tianjin 300072, China

\*Corresponding author: huanggesheng@tom.com

Received March 8, 2012; accepted May 18, 2012; posted online August 16, 2012

The fourth-order dispersion coefficient of fibers are estimated by the iterations around the third-order dispersion and the high-order nonlinear items in the nonlinear Schrodinger equation solved by Green's function approach. Our theoretical evaluation demonstrates that the fourth-order dispersion coefficient slightly varies with distance. The fibers also record  $\beta_4$  values of about 0.002, 0.003, and 0.00032 ps<sup>4</sup>/km for SMF, NZDSF and DCF, respectively. In the zero-dispersion regime, the high-order nonlinear effect (higher than self-steepening) has a strong impact on the transmitted short pulse. This red-shifts accelerates the symmetrical split of the pulse, although this effect is degraded rapidly with the increase of  $\beta_2$ . Thus, the contributions to  $\beta_4$  of SMF, NZDSF, and DCF can be neglected.

OCIS codes: 190.7110, 060.4370.

doi: 10.3788/COL201210.101903.

The determination of the fourth-order dispersion coefficient is important to various applications, such as super-continuum generation<sup>[1]</sup>, generation and transmission of new regime solitons<sup>[2]</sup>, and broadband parametric amplification<sup>[1]</sup>, among others.

In ultra-high speed optical communications (femtosecond pulses), there is a need to clarify the general nature of pulse broadening induced by dispersion orders higher than three<sup>[3]</sup>, because even the residual fourth-order dispersion (e.g., small dispersion) causes significant broadening in extremely short pulses<sup>[4]</sup>. The analytical expressions that describe pulse shape (i.e., Gaussian pulse and interference) at the receiver in the presence of  $n$ th order dispersion have been reported in Ref. [5].

Chromatic dispersion (CD) is determined by taking advantage of the interplay between dispersion and nonlinear effects, such as measuring the parametric four-wave mixing (FWM) conversion efficiency<sup>[6]</sup> or the modulation instability (MI) sidebands<sup>[7]</sup>. Both methods fundamentally rely on phase-matching condition that, in turn, depends on the dispersion coefficients and pump power; thus, the pump power should be high (>1 W) to achieve parametric amplification<sup>[8]</sup>. A method has been proposed to measure  $\beta_4$  using a low-power tunable laser and low-power amplified spontaneous emission (ASE) noise source, which directly provides the ratio of  $\beta_3/\beta_4$ <sup>[9]</sup>. Scaling the MI emitted by soliton fission in the normal dispersion regime facilitates the retrieval of the fourth-order dispersion coefficient<sup>[10]</sup>. The FWM method for short, highly nonlinear fibers has been introduced and validated experimentally<sup>[11]</sup>. This method measures ultra-low values of the fourth-order dispersion coefficient.

This letter presents a theoretical estimation of the fourth-order dispersion coefficient, which is based on the iteration method related to high-order dispersion and nonlinear items as well as the Green function solution of nonlinear Schrodinger equation (NLSE). The values of  $\beta_4$  slightly vary with the distance in some experiment results, but this estimation does not require pulse power and fiber parameters. The high-order nonlinear effect that is higher than self-steepening does not generate dis-

tinct impact on the transmitted pulse in the conventional fibers (SMF, DCF, and NZDSF). However, the impact on zero-dispersion regime or high nonlinear fibers cannot be ignored.

The NLSE that governs the wave transmission in fibers is given by

$$\frac{\partial u}{\partial z} + \frac{i}{2}\beta_2 \frac{\partial^2 u}{\partial t^2} - \frac{1}{6}\beta_3 \frac{\partial^3 u}{\partial t^3} - i\gamma \exp(-2\alpha z) \cdot \left[ |u|^2 u + is \frac{\partial |u|^2}{\partial t} u + is |u|^2 \frac{\partial u}{\partial t} \right] = 0, \quad (1)$$

where  $\beta_2$  and  $\beta_3$  are the CDs,  $\gamma$  is the nonlinear coefficient,  $s$  is the self-steepening parameter, and  $\alpha$  is the fiber loss. The solution in the frequency domain is given by

$$u(z + dz, \omega) = \exp(dz\hat{D}) \exp(dz\hat{N})u(z, \omega), \quad (2)$$

where  $\hat{D} = \frac{i}{2}\omega^2\beta_2 - \frac{i}{6}\omega^3\beta_3$  and  $\hat{N} = \Gamma\{i\gamma \exp(-2\alpha z) [|u|^2 + is \frac{\partial |u|^2}{\partial t} + is |u|^2 \frac{\partial}{\partial t}]\}$ , in which  $\Gamma$  represents the Fourier transform.

If  $\hat{L} = \frac{\partial}{\partial z} - \hat{D} - \hat{N}$  and  $\hat{L}G(z, z', \omega) = \delta(z - z')$ , we obtain the Green function as

$$G(z, z', \omega) = \frac{1}{2\pi} \int_{-\infty}^{+\infty} \frac{\exp[-ik(z - z')]}{ik - \hat{D} - \hat{N}} dk. \quad (3)$$

In constructing the iteration given by

$$\beta_3 = \beta_3^0 + \delta\beta_3, \quad u(z, \omega) = u^0(z, \omega) + \delta u(z, \omega),$$

then,

$$\delta u(z, \omega) = \int G(z, z', \omega) Z(z', \omega, \delta\beta_3(z'), u^0(z', \omega)) dz', \quad (4)$$

where  $Z(z', \omega, \delta\beta_3(z'), u^0(z', \omega)) = -\frac{i}{6}\delta\beta_3(z')\omega^3 u^0(z', \omega)$ , and  $u^0(z', \omega, \beta_3^0)$  is determined by Eq. (2). The minimum value of  $\delta u(z, \omega)$  satisfies  $\partial \delta u(z, \omega) / \partial \omega = 0$ ,  $R[\partial^2 \delta u(z, \omega) / \partial \omega^2] > 0$ ; therefore,

$$\delta\beta_3 = \exp \left[ \int_{-\infty}^{+\infty} \left( -\frac{1}{G} \frac{\partial G}{\partial \omega} - \frac{3}{\omega} - \frac{1}{u^0} \frac{\partial u^0}{\partial \omega} \right) d\omega \right]. \quad (5)$$

Next, we obtained the high-order nonlinear effect into account by constructing another iteration related to  $\delta\gamma$  given by

$$\gamma = \gamma^0 + \delta\gamma, u(z, \omega) = u^0(z, \omega) + \delta u(z, \omega).$$

This process was repeated through which we obtain

$$\delta\gamma \approx \exp \left[ \int_{-\infty}^{+\infty} \left( -\frac{1}{G} \frac{\partial G}{\partial \omega} - \frac{3is}{1-3is\omega} - \frac{1}{u^0} \frac{\partial u^0}{\partial \omega} \right) d\omega \right]. \quad (6)$$

Afterwards, we simulated the pulse shape affected by the high-order dispersion and nonlinear effects. Assuming  $L_D = t_0^2/|\beta_2|$  and  $u(0, t) = \int_{-\infty}^{+\infty} u(0, \omega) \exp(-i\omega t) d\omega = u_0 \exp(-t^2/t_0^2/2)$ . First, we determined the equations induced by  $\delta\beta_3$  and  $\delta\gamma$ . To extrude their impact, we chose other parameters for small values in Figs. 1 and 2. The deviation between the red and the black lines in Fig. 1(a) indicates the impacts of  $\delta\beta_3$  and  $\delta\gamma$ , that is, they induced the symmetrical split of the pulse. This split does not belong to the SPM-induced broadening oscillation spectral or  $\beta_3$ -induced oscillation in the tailing edge of the pulse, because  $\gamma$  is very small in Eq. (1) and  $\beta_3 = 0$ <sup>[12]</sup>. The self-steepening effect attributed to  $is\partial(|u|^2 u)/\partial t$  is also shown explicitly in the black line of Fig. 1(a). The symmetry of the split pulse is improved when we reduced the  $s$  value to 0.0001 in Fig. 1(b).

Is the pulse split in Fig. 1(a) caused by  $\delta\beta_3$  or  $\delta\gamma$ . The red lines in Fig. 2 describing the pulse evolutions affected by very small second-order dispersion and nonlinear (including self-steepening) coefficients, clearly demonstrate that  $\delta\beta_3$  induces the symmetrical split of the pulse. Moreover, the maximum peaks of split pulse alter vary from the spectral central to the edge and to the center. Therefore, this effect is equal to that of the fourth-order dispersion  $\beta_4$ <sup>[3,8,12]</sup>.

The impact of  $\delta\gamma$  can also be detected based on the deviation between the red and black lines in Fig. 2. This deviation accelerates pulse split when the self-steepening effect is ignored ( $s = 0$  in Fig. 2(a)), which is similar to the self-phase modulation broadening spectral and oscillation. The high nonlinear  $\gamma$  accelerating pulse split has been validated<sup>[11,13]</sup>. If  $s \neq 0$  (Fig. 2(b)),  $\delta\gamma$  simultaneously leads to split pulse redshift.

Generally, we did not take  $\delta\gamma$  into account. Thus, we clarified the case where it created impact. The red lines in the comparison between (c) with (b) in Fig. 2 do not show significant change, indicating that  $\delta\beta_3$  is slightly related to  $\gamma$ . However, the increase of  $\gamma$  (Fig. 2(c)) also increased the split pulse redshift. This means that  $\delta\gamma$  is

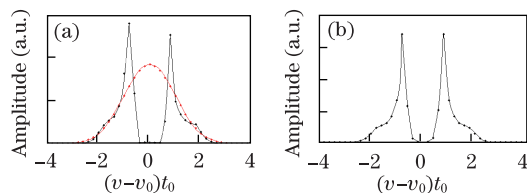


Fig. 1. (Color online) Pulse shapes with (black) and without (red)  $\delta\beta_3$  and  $\delta\gamma$ .  $\nu = \omega/2\pi$ ,  $\beta_3^0 = 0$  ps<sup>3</sup>/km,  $\gamma = 1.3 \times 10^{-4}$  km<sup>-1</sup> · W<sup>-1</sup>,  $t_0 = 80$  fs,  $z = 3.7 \times t_0^2/|\beta_2|$ ,  $\beta_2 = -21.7/150$  ps<sup>2</sup>/km,  $u_0 = |\beta_2|/\gamma/t_0^2$ .  $s =$  (a) 0.01 and (b) 0.0001.

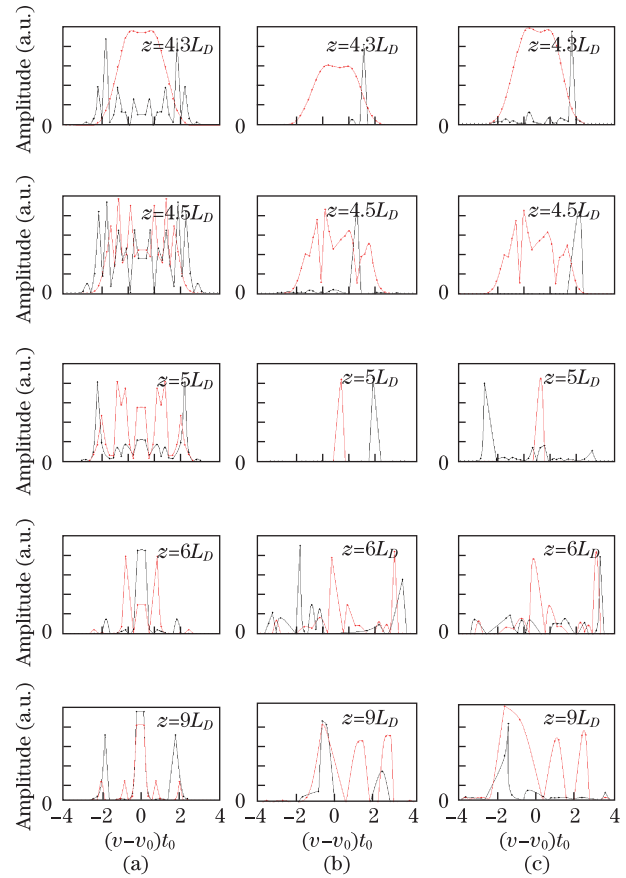


Fig. 2. (Color online) Pulse evolutions. Red line: without  $\delta\gamma$ ; black line: with  $\delta\beta_3$  and  $\delta\gamma$ . (a)  $s = 0$ ,  $\gamma = 1.3 \times 10^{-4}$  km<sup>-1</sup> · W<sup>-1</sup>; (b)  $s = 0.01$ ,  $\gamma = 1.3 \times 10^{-4}$  km<sup>-1</sup> · W<sup>-1</sup>; (c)  $s = 0.01$ ,  $\gamma = 1.3$  km<sup>-1</sup> · W<sup>-1</sup>. Other parameters are the same as those shown in Fig. 1.

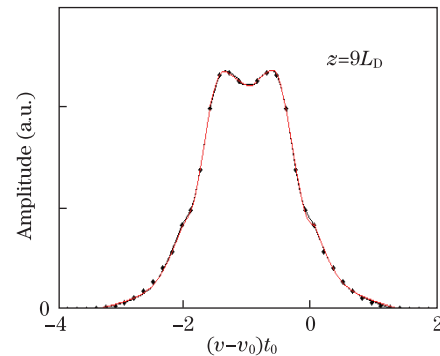


Fig. 3. Pulse shapes with and without  $\delta\gamma$ .  $\beta_2 = -21.7$  ps<sup>2</sup>/km,  $s = 0.01$ ,  $\gamma = 1.3$  km<sup>-1</sup> · W<sup>-1</sup>. Other parameters are the same as those shown in Fig. 2.

related to  $\gamma$ , and a high nonlinear coefficient strengthens the impact of  $\delta\gamma$ . In addition, the pulse does not split until  $z = 9L_D$  and the black line (with  $\delta\gamma$ ) is completely overlapped with the red line (without  $\delta\gamma$ ) (Fig. 3). This results in the higher second-order dispersion  $\beta_2$  causing an impact on covered  $\delta\gamma$  that, in turn, weakens the impact of  $\delta\beta_3$ . Therefore,  $\delta\gamma$  should be taken into account when simulating pulse shape in the zero-dispersion regime or the high nonlinear coefficient fibers.

Therefore, we utilized  $\delta\beta_3$  to determine the fourth-order dispersion coefficient  $\beta_4$ . Fiber parameters are

listed in Table 1. The process is shown in Fig. 4 and the dispersion operator that includes  $\beta_4$  is given by

$$\hat{D} = \frac{i}{2}\omega^2\beta_2 - \frac{i}{6}\omega^3\beta_3 + \frac{i}{24}\omega^4\beta_4.$$

We plotted the fourth-order dispersion coefficients of SMF, NZDSF, and DCF (Fig. 5). The  $\beta_4$  averages are listed in Table 2. These average values are different from those determined by the FWM or MI effect, where  $\beta_4$  relies on power and broadening frequency<sup>[11,13]</sup>. Here, the colored dotted lines are slightly separated; thus, our method shows that the fourth-order dispersion is also a function of distance, and every type of fiber has its special average  $\beta_4$ , revealing the characteristic of fibers. These values are similar to the experiment results in high nonlinear fibers<sup>[11,13]</sup>. Although we consider the high-order nonlinear effect  $\delta\gamma$ , the items  $is\delta\gamma\partial(|u|^2u)/\partial t$  and  $i\delta\gamma\exp(-2\alpha z)|u|^2u$  have small contributions to  $\beta_4$  at only  $10^{-26}$  ps<sup>4</sup>/km quantity order for the typical SMF. Here, the impact of  $\delta\gamma$  is hidden by the relatively strong  $\beta_2$ . However, our calculation of  $\beta_4$  remains bigger than the experiment results<sup>[11,13]</sup>. This result is attributed to the dependency of  $\beta_4$  on frequency. Furthermore, the self-steepening effect  $is\partial(|u|^2u)/\partial t$  apparently affects the pulse. If this effect is ignored,  $\beta_4$  becomes as low as the experimental results<sup>[11,13]</sup>.

In conclusion, the fourth-order dispersion coefficient

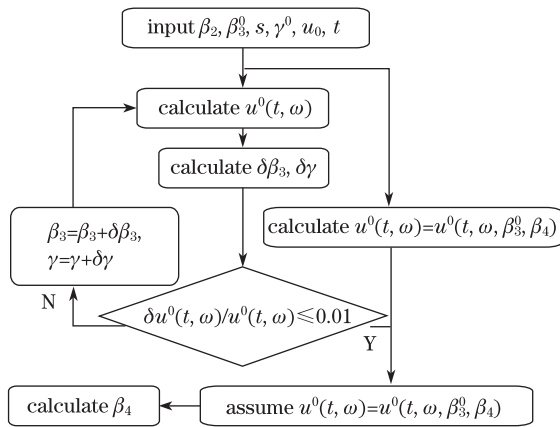


Fig. 4.  $\beta_4$  calculations.

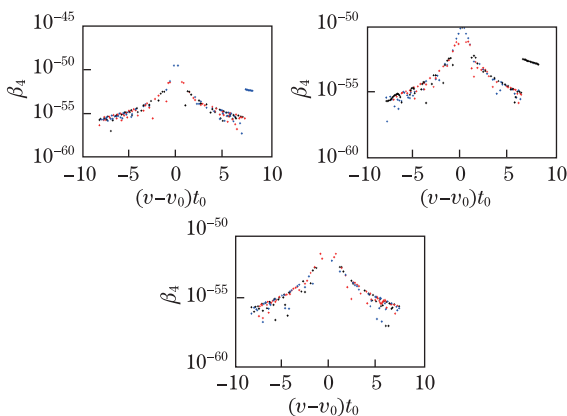


Fig. 5. (Color online)  $\beta_4$  in SMF, NZDSF and DCF, respectively. Black line:  $z = 1.5L_D$ ; red line:  $z = 5L_D$ ; blue line:  $z = 50L_D$ . Parameters are listed in Table 1.

Table 1. Fiber Parameters

	DCF	NZDSF	SMF
$a$ (dB/km)	0.59	0.21	0.21
$\gamma$ (km <sup>-1</sup> · W <sup>-1</sup> )	5.5	2.2	1.3
$s$	0.01	0.01	0.01
$\beta_2$ (ps <sup>2</sup> /km)	110	-5.6	-21.7
$\beta_3$ (ps <sup>3</sup> /km)	-0.5	0.115	0.1381
Central Wavelength (nm)	1 550	1 550	1 550

Table 2.  $\beta_4$  Average Values. Units: ps<sup>4</sup>/km

	$Z = 1.5L_D$	$Z = 5L_D$	$Z = 50L_D$
DCF	0.0003	0.00035	0.00032
NZDSF	0.0022	0.003	0.0032
SMF	0.0012	0.002	0.0025

is estimated by theory simulations based on Green's function approach and the iteration method, including the high-order nonlinear effect (higher than self-steepening). The high-order nonlinear effect induces strong pulse split and redshift in the zero-dispersion regime. However, this impact is rapidly degraded by  $\beta_2$  increase. Therefore, the impact of conventional fibers on  $\beta_4$  can be neglected (only  $10^{-26}$  ps<sup>4</sup>/km quantity order for the typical SMF). Our simulation values are consistent with some reported experiment results, wherein  $\beta_4$  varies with distance. However, we delete the high-order nonlinear effect from  $\beta_4$ . The  $\beta_4$  values for SMF, NZDSF, and DCF are about 0.002, 0.003, and 0.00032 ps<sup>4</sup>/km, respectively.

## References

1. J. M. Chávez Boggio, S. Tenenbaum, and H. L. Fragnito, *J. Opt. Soc. Am. B* **24**, 1428 (2001).
2. M. E. Marhic, N. Kagi, T.-K. Chiang, and L. G. Kazovsky, *Opt. Lett.* **21**, 573 (1996).
3. J. Capmany, D. Pastor, S. Sales, and B. Ortega, *Opt. Lett.* **27**, 960 (2002).
4. J. Zhang and C. Dai, *Chin. Opt. Lett.* **3**, 295 (2005).
5. A. Panajotovic, D. Milovic, and A. Mitic, in *Proceedings of TELSIS 2005* 547 (2005).
6. H. Chen, *Opt. Commun.* **220**, 331 (2003).
7. J. Fatome, S. Pitois, and G. Millot, *Opt. Fiber Technol.* **12**, 243 (2006).
8. K. Igarashi, S. Saito, M. Kishi, and M. Tsuchiya, *IEEE J. Sel. Topics Quantum Electron.* **8**, 521 (2002).
9. J. M. C. Boggio and H. L. Fragnito, *J. Opt. Soc. Am. B* **24**, 2046 (2007).
10. B. Auguie, A. Mussot, A. Boucon, E. Lantz, and T. Sylvestre, *IEEE Photon. Technol. Lett.* **17**, 1825 (2006).
11. F. Gholami, J. M. C. Boggio, S. Moro, N. Alic, and S. Radic, in *Proceedings of IEEE Photonics Society Summer Topical Meeting Series* 162 (2010).
12. G. P. Agrawal, *Nonlinear Fiber Optics*, in *Optics and Photonics* (Academic, San Diego, 2001).
13. M. E. Marhic, K. K. Y. Wong, and L. G. Kazovsky, *IEEE J. Sel. Topics Quantum Electron.* **10**, 1133 (2004).